Frustrated Ising model on the Cairo pentagonal lattice

M. Rojas, Onofre Rojas, and S. M. de Souza
Departamento de Ciencias Exatas, Universidade Federal de Lavras, C.P. 3037, 37200-000 Lavras, Minas Gerais, Brazil
(Received 25 May 2011; published 16 November 2012)

Through the direct decoration transformation approach, we obtain a general solution for the pentagonal Ising model, showing its equivalence to the isotropic free-fermion eight-vertex model. We study the ground-state phase diagram, in which one ferromagnetic (FM) state, one ferrimagnetic (FIM) state, and one frustrated state are found. Using the exact solution of the pentagonal Ising model, we discuss the finite-temperature phase diagrams and find a phase transition between the FIM state and the disordered state as well as a phase transition between the disordered state and the FM state. We also discuss some additional remarkable properties of the model, such as the magnetization, entropy, and specific heat, at finite temperature and at its low-temperature asymptotic limit. Because of the influence of the second-order phase transition between the frustrated and ferromagnetic phases, we obtain surprisingly low values of the entropy and the specific heat until the critical temperature is reached.

DOI: 10.1103/PhysRevE.86.051116 PACS number(s): 05.50.+q, 05.10.−a, 75.10.Hk, 64.60.De

I. INTRODUCTION

Over the past six decades, much effort has been devoted to determining the critical behavior of statistical properties of lattice models, which would allow a deeper understanding of order-disorder phenomena in magnetic solids. Following Onsager's pioneering exact solution for the square lattice Ising model [1], exact solutions were also obtained for other regular two-dimensional lattice structures [2]. In particular, exact results have been attained for the triangular, honeycomb, kagome, and bathroom-tile lattices [3–5], as well as for two-dimensional models, such as the Union Jack (centered square) [6] and the square kagome [7] lattices.

Geometrical frustration is mainly based on the triangle and tetrahedron structures, but it was also found in the Ising model on a pentagonal Penrose lattice proposed by Waldor *et al.* [8] and solved exactly using the transfer matrix approach. More recently Urumov [9] considered the Ising model on the Cairo pentagonal lattice using the decoration transformation [10]. This model has been mapped onto the Union Jack lattice [6] and its critical temperature and spontaneous magnetization properties have been discussed. This model is interesting from a mathematical point of view. A few years ago, real materials with a Cairo pentagonal lattice structure were found; for example, the Fe^{3+} lattice in $Bi_2Fe_4O_9$ (described as a pentagonal Heisenberg model) was discussed by Ressourche *et al.* [11]. This material shows magnetic frustration. Also, theoretical calculations of the phonon structure of antiferromagnetic $Bi_2Fe_4O_9$ (space group $Pbnm$ No. 55, $T \approx 240$ K) were studied using lattice dynamics and these results were confirmed experimentally by polarized Raman spectroscopy from 10 to 300 K [12]. More recently, some additional experimental studies were performed [13,14]. Ralko [15] also discussed the hard-core extended boson Hubbard model on the Cairo pentagonal lattice, using the numerical quantum Monte Carlo study of stochastic series expansion and cluster mean-field theory.

The purpose of this paper is to present a general exact solution of the pentagonal Ising model and as a special case we obtain the Urumov solution using a standard decoration transformation approach [10]. Furthermore, we present a more simplified solution through the direct decoration transformation [16] instead of the standard one [10]. The generalized version of the latter [17,18] is widely used to solve some two-dimensional decorated Ising [19] and Ising-Heisenberg [20–22] models.

This paper is organized as follows. In Sec. II we consider the detailed description of the Ising model on the Cairo pentagonal lattice. In Sec. III we discuss its phase diagram at zero temperature. Section IV is devoted to the pentagonal Ising model mapping, using the direct decoration transformation [16] for the isotropic free-fermion vertex model [23], presenting the most relevant results and discussion. In Sec. V we obtain the finite-temperature phase diagrams, critical temperature, magnetization, entropy, and specific heat. Section VI summarizes our discussion.

II. ISING MODEL ON THE CAIRO PENTAGONAL LATTICE

The highly anisotropic Heisenberg model on the Cairo pentagonal lattice considered by Ressourche *et al.* [11] could be reduced to the Ising model on a Cairo pentagonal lattice. Therefore, let us consider the Ising model on a planar lattice where the tiling is achieved with nonregular pentagons; the lattice may be viewed as an assembly of checkerboard ordering with the elementary cell (see Fig. 5) rotated by $\pi/2$ in the neighboring square plaquettes, as shown in Fig. 1 (for more details see Ref. [9]).

The Hamiltonian of the Cairo pentagonal Ising model (represented schematically in Fig. 1), discussed previously by Urumov [9], is expressed by

$$H = -J_1 \sum_{\langle i,j \rangle} s_i s_j - J \sum_{\langle k,l \rangle} s_k \tau_l, \tag{1}$$

where the first summation is the contribution of the interaction between the nearest neighbor with spin s_i (s_i interacting with coordination number 3) and J_1 corresponds to the interaction between s_i and s_j. While the second summation is the contribution of the nearest-neighbor interaction J between spin s_k and spin τ_l (τ_l's interacting with coordination number 4), conveniently we assume $s_i = \pm 1$ and $\tau_l = \pm 1$.

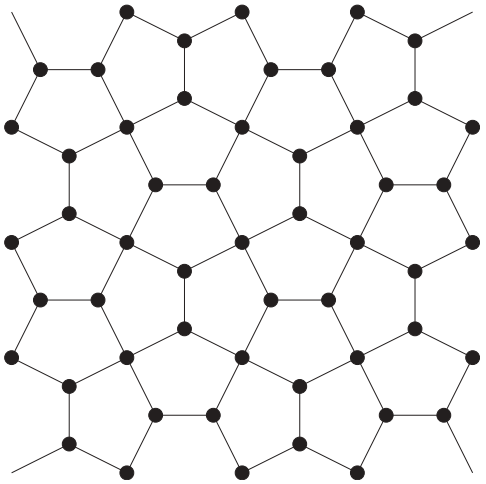

FIG. 1. Schematic representation of the Cairo pentagonal lattice.

III. PHASE DIAGRAM AT ZERO TEMPERATURE

In this section we discuss the phase diagram at zero temperature of the Hamiltonian given in Eq. (1). In order to discuss the phase diagram at zero temperature, we define the magnetization M for the pentagonal lattice that is used throughout the paper, given by

$$M = \frac{M_0 + 2M_1}{3}, \tag{2}$$

with $M_0 = \langle \tau_1 \rangle$ and $M_1 = \langle s_1 \rangle$.

The energy per plaquette of three ground states that appear for the pentagonal lattice Ising model is expressed in terms of an elementary cell (see Fig. 5). It is worth highlighting that the elementary cell should not be confused with the unit cell of the pentagonal lattice.

(i) The ferromagnetic (FM) state or saturated state has a total magnetization $M = 1$ and ground-state energy per plaquette $E = -J_1 - 4J$. Thus the FM state can be represented as

$$|\mathrm{FM}\rangle = \left|\begin{smallmatrix} + & + & + \\ + & + & + \end{smallmatrix}\right\rangle. \tag{3}$$

This state is limited by $J > 0$ for $J_1 > 0$ and $J_1 > -J$ for $J_1 < 0$, as displayed in Fig. 2.

(ii) The ferrimagnetic state (FIM) has a total magnetization $M = 1/3$ and ground-state energy per plaquette $E = -J_1 + 4J$, which corresponds to the configuration displayed in Fig. 2. Analogous to the previous case, we describe the state by

$$|\mathrm{FIM}\rangle = \left|\begin{smallmatrix} + & - & + \\ + & - & + \end{smallmatrix}\right\rangle. \tag{4}$$

This state is limited by $J < 0$ for $J_1 > 0$ and $J_1 > J$ for $J_1 < 0$, as illustrated in Fig. 2.

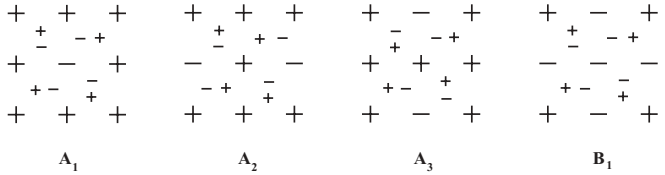

FIG. 2. Phase diagram at zero temperature of the pentagonal Ising model.

(iii) The frustrated state (FRU) is given as a combination of states $\left|\begin{smallmatrix} \sigma & \sigma & \sigma \\ \sigma & - & \sigma \end{smallmatrix}\right\rangle$ with its rotated elementary cell and spin inversion on the elementary cell with ground-state energy per plaquette $E = J_1 - 2|J|$, which can be expressed by

$$|\mathrm{FRU}\rangle = \text{combinations of } \left\{\left|\begin{smallmatrix} + & + & + \\ + & - & \end{smallmatrix}\right\rangle, \left|\begin{smallmatrix} - & - & - \\ - & + & \end{smallmatrix}\right\rangle\right\}. \tag{5}$$

This state is limited by $J_1 \leqslant -|J|$ (see Fig. 2).

We define m as the magnetization for each frustrated-state configuration in the range between $m = -1/6$ and $1/6$ (we denote by M the average of total magnetization). Combining the state of the elementary cell displayed in Eq. (5) and its rotation in $\pi/2$ of the elementary cell, it is possible to generate the geometrically frustrated state. In particular, when we combine half states $\left|\begin{smallmatrix} + & + & + \\ + & - & \end{smallmatrix}\right\rangle$ and the remaining states with $\left|\begin{smallmatrix} - & - & - \\ - & + & \end{smallmatrix}\right\rangle$, we obtain an antiferromagnetic state, with null total magnetization. Other intermediate states with magnetization $0 \leqslant m \leqslant 1/6$ also could be obtained by combining the elementary cell state with different relative amounts of the state given by Eq. (5). More specifically, the unit cell magnetization could be classified as displayed in Fig. 3, i.e., A_i $(i = 1,2,3)$ and B_1, with magnetization $m = 1/6$ and $-1/6$, respectively. Certainly, this is not the only way to classify the unit cell by its magnetization; any other classifications of the unit cell lead us to the same kind of lattice configuration. In Fig. 4 we show two particular situations of such a lattice configuration, formed by the unit cells of type A_i and B. In the bulk limit we have a lattice with total magnetization $1/6$. In Fig. 4(b) the lattice is composed of unit cells A_2 and B_1 with a different concentration, generating a different total magnetization of the lattice. Thus we obtain the total magnetization of each

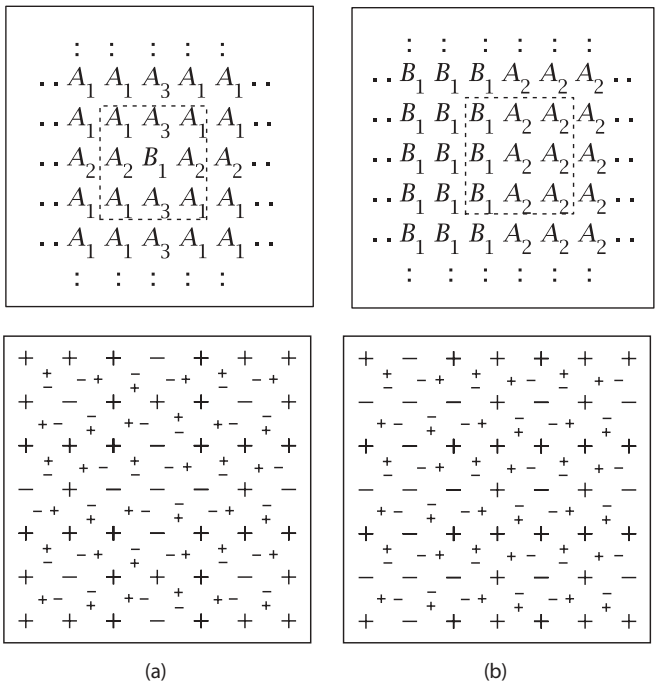

FIG. 3. Unit cells A_i $(i = 1,2,3)$ with magnetization $M = 1/6$ and unit cell B_1 with $M = -1/6$.

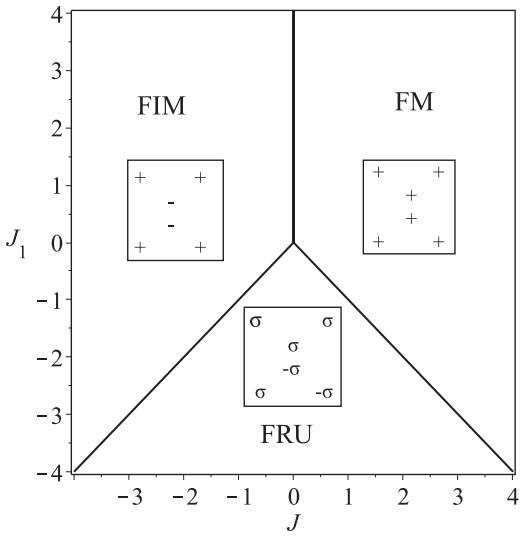

FIG. 4. (a) In the top (left) panel, we illustrate schematically an arbitrary lattice configuration, which is included in a frustrated state; the dashed square is shown explicitly in the panel below. (b) In the top (right) panel, we assemble a lattice with two different unit cells $A(m = 1/6)$ and $B(m = -1/6)$. In the panel below, the sublattice (the dashed square) is explicitly shown; the contributions of unit cells A and B are in different concentrations.

particular configuration. However, the average magnetization of all these configurations with equal energy will be null $M = 0$ of the frustrated state in the interval $-1/6 < m < 1/6$.

IV. PENTAGONAL ISING MODEL MAPPING

Through the direct decoration transformation [16], it is shown that the pentagonal Ising model is equivalent to a Union Jack lattice, which is in turn mapped onto the isotropic free-fermion eight-vertex model [24,25]. From this equivalence we can obtain the thermodynamics of the pentagonal Ising model. In order to study the spin-1/2 Ising model on a pentagonal lattice, we introduce the notation for each elementary square plaquette depicted in Fig. 5 (this should not be confused with the unit cell). In this case we assume $\{\tau_1,\tau_2,\tau_3,\tau_4\} = \pm 1$, $\{s_1,s_2\} = \pm 1$, and $\sigma = \pm 1$.

The Hamiltonian for an elementary plaquette as displayed in Fig. 5 is given by

$$-\beta H_e = J_1' s_1 s_2 + J'[s_1(\tau_1 + \tau_2) + s_2(\tau_3 + \tau_4)], \qquad (6)$$

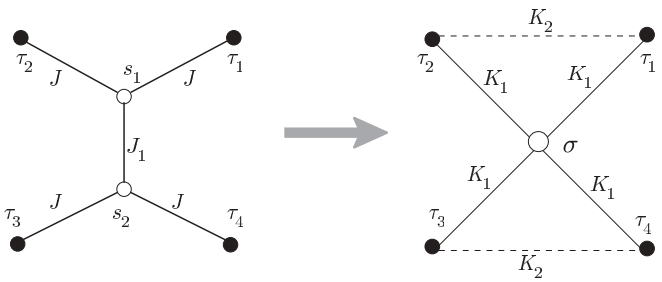

FIG. 5. Schematic representation of the elementary plaquette and its mapping to the Union Jack lattice.

where we are assuming $J_1' = \beta J_1$ and $J' = \beta J$ and β is defined by $\beta = 1/k_B T$, with k_B the Boltzmann constant and T the absolute temperature. Instead of applying the standard decoration transformation [10,17] as applied by Urumov [9], we apply the direct decoration transformation [16] to transform the plaquette into the Union Jack lattice [6]. In this case the Hamiltonian associated with the Union Jack lattice can be expressed by

$$-\beta \tilde{H}_e = K_0' + K_1'\sigma(\tau_1 + \tau_2 + \tau_3 + \tau_4) + K_2'(\tau_1\tau_2 + \tau_3\tau_4). \qquad (7)$$

The Boltzmann weights of the Hamiltonian (6) may be written

$$w(\{\tau\}) = \sum_{s_1,s_2=\pm 1} e^{J_1' s_1 s_2 + J'[s_1(\tau_1+\tau_2)+s_2(\tau_3+\tau_4)]}, \qquad (8)$$

where $\{\tau\}$ denotes the set of variables $\{\tau_1,\tau_2,\tau_3,\tau_4\}$, whereas the Boltzmann weights for the transformed plaquette is given by the relation

$$\tilde{w}(\{\tau\}) = \sum_{\sigma=\pm 1} e^{K_0' + K_1'\sigma(\tau_1+\tau_2+\tau_3+\tau_4) + K_2'(\tau_1\tau_2+\tau_3\tau_4)}. \qquad (9)$$

Similar to the previous notation, here we consider $K_0' = \beta K_0$, $K_1' = \beta K_1$, and $K_2' = \beta K_2$, where K_0' is taken as a constant shift energy, K_1' is the interaction parameter between the internal spin σ and each spin τ, and K_2' is the coupling term between spins τ.

Using the direct decoration transformation proposed in Ref. [16], we need to impose the condition $w(\{\tau\}) = \tilde{w}(\{\tau\})$ between Eqs. (8) and (9) for arbitrary τ. Therefore, we obtain only four nonequivalent configurations $\{\tau_1,\tau_2,\tau_3,\tau_4\} = \{+,+,+,+\}$, $\{+,+,+,-\}$, $\{+,+,-,-\}$, and $\{+,-,+,-\}$; any other permutation or spin inversion falls onto one of these configurations. Thus the Boltzmann weight for each configuration is given by

$$\xi_1 = w(+,+,+,+) = 2e^{K_0'+2K_2'}\cosh(4K_1'), \qquad (10)$$

$$\xi_2 = w(+,-,+,-) = 2e^{K_0'-2K_2'}, \qquad (11)$$

$$\xi_3 = w(+,+,-,-) = 2e^{K_0'+2K_2'}, \qquad (12)$$

$$\xi_5 = w(+,+,+,-) = 2e^{K_0'}\cosh(2K_1'), \qquad (13)$$

where $\xi_2 = \xi_4$ and $\xi_5 = \xi_6 = \xi_7 = \xi_8$.

The above equations satisfy the isotropic free-fermion condition [23] $w_1w_2 + w_3w_4 = w_5w_6 + w_7w_8$, following the eight-vertex model with Boltzmann weights $\omega_1,\ldots,\omega_8$ (ω should not be confused with w) displayed in Fig. 6. Hence the free-fermion condition may be rewritten in terms of ξ as

$$2\xi_5^2 = (\xi_1 + \xi_3)\xi_2. \qquad (14)$$

Therefore, the Boltzmann factor of an effective Union Jack lattice can be expressed in terms of the pentagonal Ising model

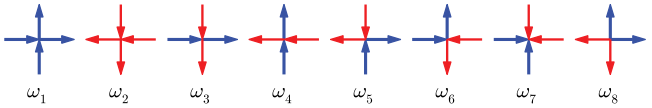

FIG. 6. (Color online) Eight-vertex model diagrams.

coupling parameters

$$\xi_1 = ru^{-4} + 2r^{-1} + ru^4, \tag{15}$$

$$\xi_2 = 2(r + r^{-1}), \tag{16}$$

$$\xi_3 = 2r + r^{-1}u^{-4} + r^{-1}u^4, \tag{17}$$

$$\xi_5 = (r + r^{-1})(u^2 + u^{-2}). \tag{18}$$

For simplicity we used the notation $r = e^{J_1'}$ and $u = e^{J'}$.

Due to the step by step decoration transformation performed by Urumov [9] (see Fig. 2), J_1 was restricted only to $J_1 > 0$ or $r > 1$ (ferromagnetic); otherwise, if we consider $J_1 < 0$, we get a imaginary parameter in the intermediate transformation proposed by Urumov. However, using the direct decoration transformation, we do not have such a restriction (Fig. 5), but only $r > 0$, which means that J_1 exchange coupling could be ferromagnetic or antiferromagnetic.

Hence the pentagonal Ising model is completely equivalent to the Ising model on the Union Jack lattice [6] with the isotropic nearest-neighbor interactions defined by K_1 and noncrossing diagonal interactions between the second nearest neighbor given by K_2. In contrast, the Union Jack lattice was mapped onto the isotropic free-fermion eight-vertex model [23] by Choy and Baxter [24]. Therefore, we relate the Boltzmann factor given by Eqs. (10)–(13) and the Boltzmann factor of the Union Jack lattice given by Eq. (4) of Ref. [24]. These relations are given by

$$\omega_1 = \frac{2\xi_1}{\sqrt{\xi_2\xi_3}}, \quad \omega_2 = \frac{2\xi_2}{\sqrt{\xi_2\xi_3}}, \quad \omega_3 = 2, \quad \omega_5 = \frac{2\xi_5}{\sqrt{\xi_2\xi_3}}. \tag{19}$$

The schematic representation of the eight-vertex model is given in Fig. 6. These Boltzmann weights will be used in the following section to study the critical temperature and spontaneous magnetization of the Cairo pentagonal Ising model.

V. THERMODYNAMICS OF THE PENTAGONAL LATTICE

In this section we discuss thermodynamical properties, such as the entropy, specific heat, and magnetization, as a function of temperature, as well as the critical temperature behavior. The thermodynamics of the pentagonal Ising model can be expressed following the results given by Fan and Wu [23]. The exact result for the free energy of the pentagonal Ising model is then given by

$$\beta f = -\frac{1}{4\pi}\int_0^{2\pi} \ln[A(\phi) + \sqrt{Q(\phi)}]d\phi, \tag{20}$$

where

$$A(\phi) = \tfrac{1}{2}\left(\xi_1^2 + \xi_2^2 + 2\xi_2\xi_3\right) + (\xi_1 - \xi_2)\sqrt{\xi_2\xi_3}\cos(\phi), \tag{21}$$

$$Q(\phi) = \left[(\xi_1 - \xi_2)\sqrt{\xi_2\xi_3}\cos(\phi) + \tfrac{1}{2}(\xi_1 + \xi_2)^2\right]^2 + \xi_1\xi_2[4\xi_2\xi_3 - (\xi_1 + \xi_2)^2]. \tag{22}$$

Once the free energy is known, we can obtain straightforwardly the critical temperature, magnetization, entropy, and specific heat.

A. Critical temperature

In order to study the spontaneous magnetization, following the result obtained by Choy and Baxter [24] and using Eq. (19), the magnetization $M_0 = \langle\tau_1\rangle$ for spins with coordination number 4 is described by

$$M_0 = 8\sqrt{1 - k^2}, \tag{23}$$

where

$$k = \frac{2\xi_2(\xi_1 + \xi_3)}{\xi_1^2 + \xi_2^2 - 2\xi_2\xi_3}. \tag{24}$$

Equation (24) is expressed in terms of the pentagonal Ising model Boltzmann factor. It is important to note that this relation is valid for arbitrary spins s_1 and s_2, as shown in Fig. 5. Using the results obtained in Ref. [24], the critical point of the Union Jack lattice is obtained from the condition $w_1 - w_2 = 2w_3$ for $w_1 > w_2$ or $w_2 - w_1 = 2w_3$ for $w_2 > w_1$; in terms of k, this means that the critical points occur at $k = 1$. Equivalently, using the pentagonal Ising model Boltzmann factor ξ, we have

$$(\xi_1 - \xi_2)^2 = 4\xi_2\xi_3. \tag{25}$$

This condition must satisfy the critical point. Rewriting Eq. (25) in terms of r and u, the critical points must satisfy the relation

$$r_c = \sqrt{2}u_c\sqrt{\frac{2u_c^6 + 2u_c^2 + \left(1 - u_c^4\right)^2\sqrt{2}}{u_c^{12} - 5u_c^8 - 5u_c^4 + 1}}, \tag{26}$$

where r_c and u_c denote r and u evaluated at the critical temperature T_c. The same expression could be obtained from Eq. (8) of Ref. [9]; however, due to the standard decoration transformation [10,17] used by Urumov [9] for this model, we have to eliminate the intermediate parameter Q. Once the intermediate parameter Q is eliminated from Eq. (8) of Ref. [9], it becomes identical to our Eq. (26) for the case of $J_1 > 0$ (ferromagnetic coupling), which was previously studied by Urumov [9].

In Eq. (26) we provide a closed expression for the critical point of the pentagonal Ising model. The curves where the critical points occur are illustrated in Fig. 7.

The finite-temperature properties of the system are investigated by considering the effect of the parameters J and

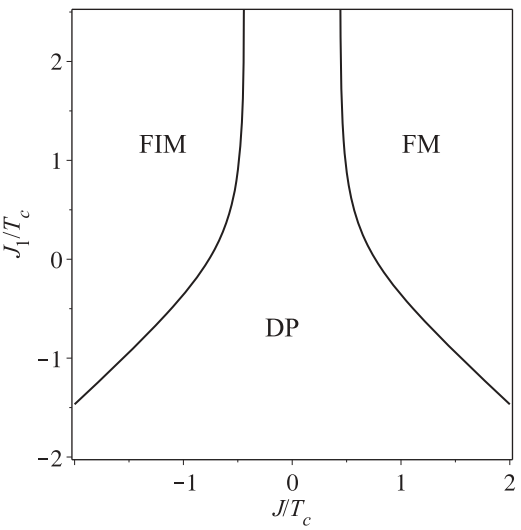

FIG. 7. Critical points curve for the pentagonal Ising model as a function of the parameters J/T_c and J_1/T_c.

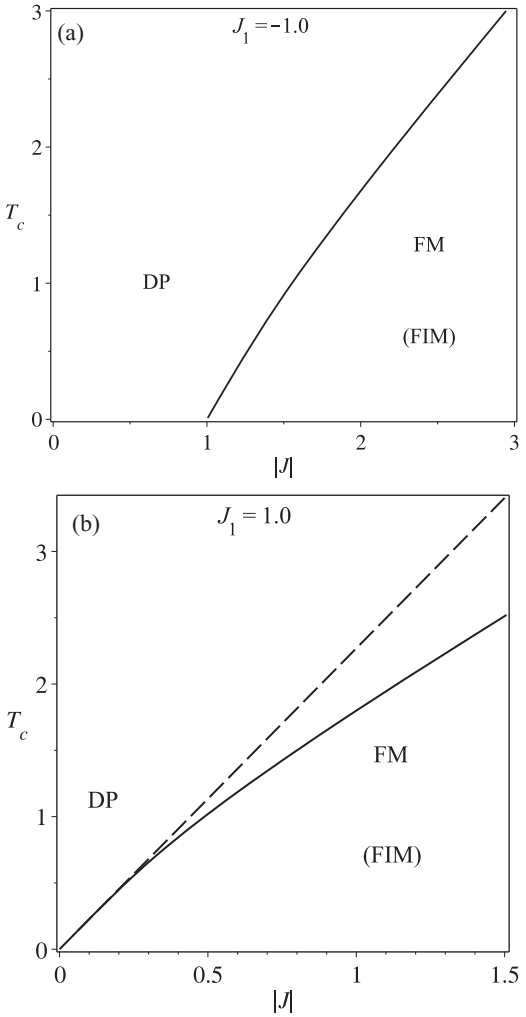

FIG. 8. Phase diagrams as a function of temperature T_c and the parameter $|J|$ for two different values of J_1. In (b) the dashed lines show the limiting values of $J \to 0$ and $T_c \to 0$.

J_1 on the critical behavior. In Fig. 7 we display the critical point regions in units of critical temperature, where the phase transitions of the FIM region to a disordered phase (DP) and a DP to a FM phase are illustrated. It is important to highlight that Fig. 7 becomes similar to Fig. 2 when $T_c \to 0$.

An alternative phase diagram is depicted in Fig. 8, where the phase diagrams are illustrated in the $(T_c, |J|)$ plane (since T_c is invariant under the $J \to -J$ exchange) for fixed parameter J_1. In Fig. 8(a) the second-order phase transition line is shown in the $(T_c, |J|)$ plane when the parameter J_1 is fixed at $J_1 = -1.0$; in this case there is a DP. Concretely, for $J < 0$ we show two regions: the FIM phase and the DP; for $J > 0$ we have a DP and a FM phase.

In Fig. 8(b) we show the behavior of the critical temperature when $J_1 = 1.0$, displayed as a solid line. For low values of $T \approx 0$, the left-hand side of Eq. (26) goes to infinity; this implies that the denominator on the right-hand side must satisfy the condition $u_c^{12} - 5u_c^8 - 5u_c^4 + 1 = 0$. Thus we obtain the solution $T_c = \pm 2.2691 J$ (dashed lines), which is valid within the limit $J \to 0$ and $T_c \to 0$. This result is in agreement with the phase diagram at zero temperature see, for instance, Fig. 2); more specifically, for $J_1 = 1$, the phase transition occurs at $J = 0$.

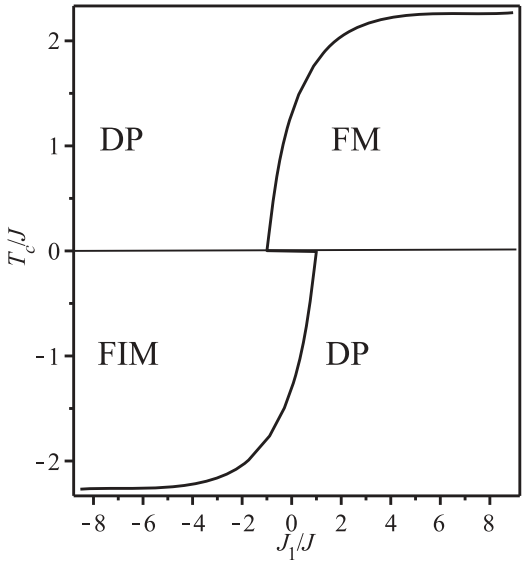

FIG. 9. Phase diagram in the $(T_c/J, J_1/J)$ plane for the pentagonal Ising model.

We now comment on the finite-temperature phase diagrams displayed in Fig. 9, in which the critical temperature T_c/J is shown as a function of the parameter J_1/J. Using the equation of the critical points (26), we obtain the plot illustrated in Fig. 9. From that we can analyze three limiting cases.

(i) For $\frac{J_1}{J} \to 0$ we obtain $T_c/J = 1.3084$ ($T_c/J = -1.3084$) and the pentagonal lattice is reduced to a ferromagnetic (ferrimagnetic, with total magnetization $M = 1/3$) decorated square lattice, respectively.

(ii) For $\frac{J_1}{J} \to \infty$, from our calculation, for $J > 0$ and $J_1 > 0$, we find the solution $T_c/J = 2.2691$; in this case the pentagonal lattice is reduced to the ferromagnetic square lattice. In the case $J < 0$ and $J_1 < 0$, in the limit under consideration ($\frac{J_1}{J} \to \infty$), the pentagonal lattice falls into the bottom right-hand corner, which is a DP state (see Fig. 9).

(iii) For $\frac{J_1}{J} \to -\infty$ we obtain $T_c/J = -2.2691$ for $J < 0$ and $J_1 > 0$ and the pentagonal lattice is reduced to a ferrimagnetic (with total magnetization $M = 1/3$) square lattice. Meanwhile, for $\frac{J_1}{J} \to -\infty$ for $J > 0$ and $J_1 < 0$ the pentagonal lattice falls into a disordered state, which corresponds to the top left corner of Fig. 9.

When $K_2 = 0$, according to a pentagonal lattice mapping onto an effective square lattice (see Fig. 5), within the limit $\frac{J_1}{J} \to \infty$, the effective lattice is reduced to a ferromagnetic square lattice. In the limit $\frac{J_1}{J} \to -\infty$ the pentagonal Ising model reduces to an antiferromagnetic square lattice.

B. Internal energy

The internal energy of the pentagonal lattice Ising model defined by $U = T^2 \frac{\partial (f/T)}{\partial T}$ can be obtained straightforwardly from Eq. (20). In Fig. 10 we display the internal energy as a function of coupling parameter J in the low-temperature limit in order to observe the low-lying energy contribution close to the critical temperature assuming $J_1 = -1.0$. The dashed line corresponds to the DP internal energy at $T = 0$ (the ground-state energy), given by $U = -1 - 2J$, while the dash-dotted line indicates the internal energy $U = 1 - 4J$

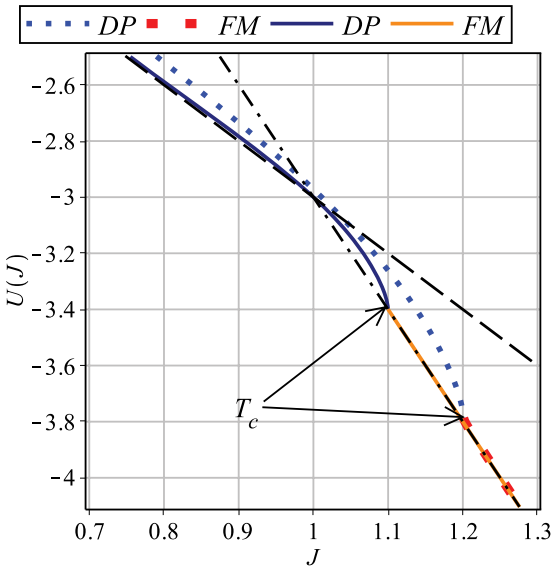

FIG. 10. (Color online) Internal energy U as a function of J for a fixed value $J_1 = -1.0$. The dashed line corresponds to the DP ground energy and the dash-dotted line corresponds to the FM ground energy.

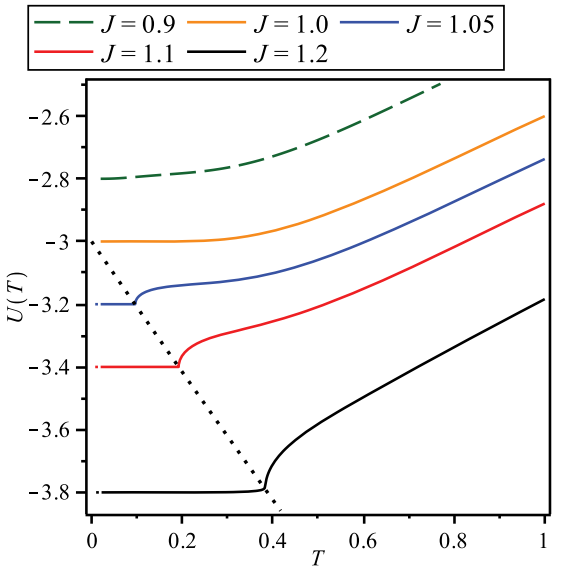

FIG. 11. (Color online) Internal energy U as a function of T and a fixed value $J_1 = -1.0$. The dotted curve corresponds to $U(T_c)$.

from which the phase transition at zero temperature occurs at $J = 1$. In the case $T_c \to 0$ and assuming $J = 1 + \delta$ with $\delta \gtrsim 0$, we have $u_c \to \infty$ and then it is possible to write $u_c = r_c^{-1-\delta}$. Further, by substituting into Eq. (26), after some algebraic manipulations we obtain $r_c^{2\delta} \approx \frac{1}{2\sqrt{2}}$, where $r_c = e^{-1/T_c}$ was defined previously. Thus a second-order phase transition occurs at $T_c \approx \frac{2(|J|-1)}{\ln(2\sqrt{2})}$. It is worth highlighting that the lowest critical temperature occurs at $T_c = 0$. Therefore, the contribution of the low-lying energy is absorbed by the second-order phase transition. Certainly there is no second-order phase transition for $J < 1$ and $J_1 = -1$. The solid blue (thick) line and the dark-blue (thin) curve represent the internal energy in the disordered phase, while by the red (thick) line and the orange (thin) line curve represent the ferromagnetic region for two critical temperatures $T_c = 0.192$ and 0.385.

In Fig. 11 we plot the internal energy as a function of temperature for several values of J around the second=order phase transition, assuming a fixed value for $J_1 = -1.0$. The black dotted line represents the internal energy $U(T_c)$ evaluated at the critical temperature T_c given by Eq. (37) at low temperature. Below the critical temperature, the internal energy is almost constant (ferromagnetic phase), which means that it is mainly given by the zero-temperature ground-state energy. Although at a critical temperature there is a sudden change of curvature, this change becomes dramatic for lower critical temperature; for higher critical temperature this change of curvature becomes smoother. The lowest critical temperature occurs at $T_c = 0$ for $J = 1$; therefore, for lower values of the coupling parameter J there is no second-order phase transition. For a sufficiently high temperature the internal energy leads to an asymptotic limit, whereas the internal energy increases almost proportionally to the temperature.

C. Spontaneous magnetization

The total magnetization M is given by Eq. (2) for the pentagonal Ising model, which will be discussed in order to show the spontaneous magnetization. It ought to be pointed out that the calculation of the magnetization of internal spin s_i, $i = 1,2$, may be obtained following the results obtained by Choy and Baxter [24], which could be expressed by the relation

$$M_1 = \langle s_1 \rangle = c_1 \langle \tau \rangle + c_2 \langle \tau_1 \tau_2 \tau_3 \rangle, \tag{27}$$

where after some algebraic manipulations the coefficients become

$$c_1 = \frac{1}{4}\left(\frac{\Sigma_1}{\xi_1} + 2\frac{\Sigma_5}{\xi_5}\right), \tag{28}$$

$$c_2 = \frac{1}{4}\left(\frac{\Sigma_1}{\xi_1} - 2\frac{\Sigma_5}{\xi_5}\right). \tag{29}$$

Defining Σ_1 and Σ_5 in analogy to the Boltzmann factors ξ, we have

$$\Sigma_1 = \frac{-2r}{u^4} + 2ru^4, \tag{30}$$

$$\Sigma_5 = \frac{-2r}{u^2} + 2ru^2. \tag{31}$$

In order to obtain the three-spin correlation function $\langle \tau_1 \tau_2 \tau_3 \rangle$ we use a checkerboard Ising model equivalent to that used by Choy and Baxter [24]. Here we use the relation obtained in Ref. [24], but in our case we rewrite this relation in terms of the pentagonal Ising model Boltzmann factor. Hence, using some algebraic manipulations we have

$$\langle \tau_1 \tau_2 \tau_3 \rangle = R(r,u) \langle \tau_1 \rangle, \tag{32}$$

where

$$R(r,u) = \frac{2\xi_1}{\xi_1 - \xi_3} + \frac{\xi_1 + \xi_3}{\xi_1 - \xi_3}\left(1 - \frac{2\xi_1\sqrt{\xi_1^2 + \xi_2^2 - 2\xi_2\xi_3}}{\xi_1^2 - \xi_2\xi_3}\right). \tag{33}$$

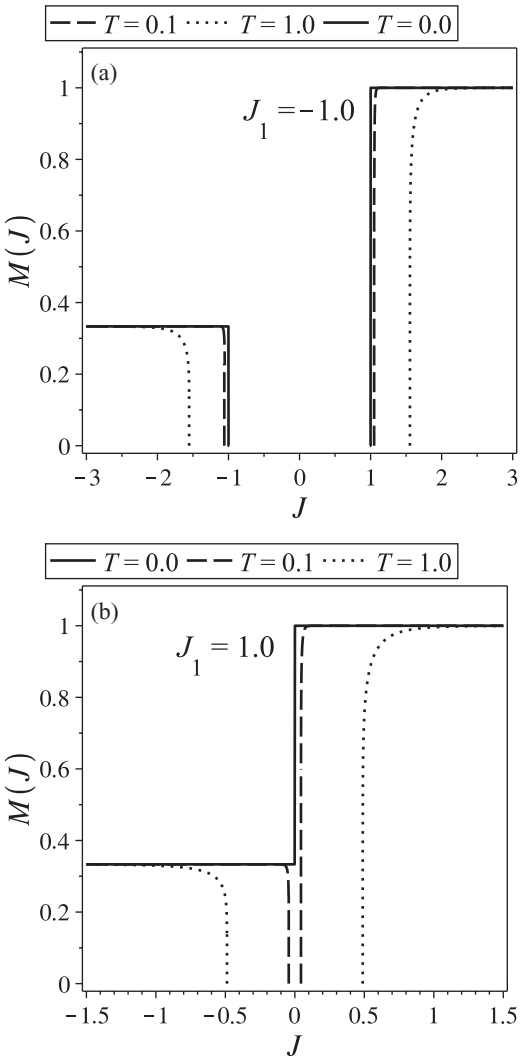

FIG. 12. Total magnetization of the pentagonal Ising model for three different values of T as a function of the parameter J and fixed parameter J_1. (a) $J_1 = -1.0$ and (b) $J_1 = 1.0$.

Therefore, the magnetization M_1 can be expressed as a function of magnetization M_0, which is given by

$$M_1 = \frac{1}{4}\left[\left(\frac{\Sigma_1}{\xi_1} + 2\frac{\Sigma_5}{\xi_5}\right) + \left(\frac{\Sigma_1}{\xi_1} - 2\frac{\Sigma_5}{\xi_5}\right) R(r,u)\right] M_0. \quad (34)$$

It is important to highlight that Eq. (34) is expressed in terms of the original parameters of the pentagonal Ising model instead of parameters of the effective Hamiltonian such as those obtained by Urumov [9]. Using Eq. (34), we are able to manipulate the parameters of the pentagonal Ising model in order to discuss the spontaneous magnetization. At the critical point we need to substitute the expression $r = r_c^{T_c/T}$, where r_c is defined in Eq. (26). From Eqs. (23) and (34) we can obtain a closed expression for the total magnetization of the Ising model on a pentagonal lattice, using the relation given by Eq. (2).

We now discuss the behavior of the total magnetization of the pentagonal Ising model as a function of the parameter J for the low-temperature limit. In Fig. 12 we plot the magnetization at low temperature as a function of J, where we display two types of plateaus for the FIM state and the FM state. This is in agreement with the phase diagram displayed in Figs. 2 and 7, whereas the intermediate state corresponds to the FRU phase and the DP, respectively.

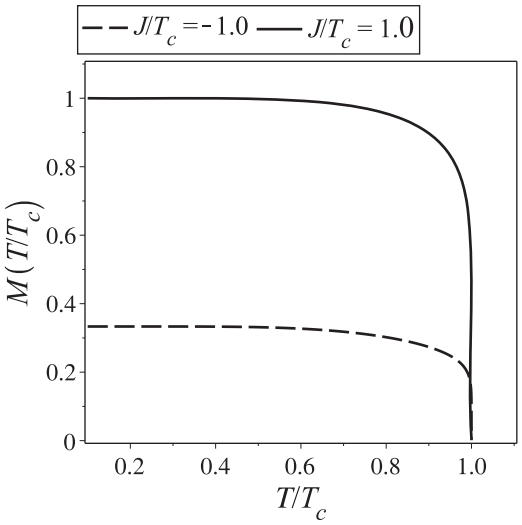

FIG. 13. Temperature dependence of the total magnetization of the pentagonal Ising model for two different values of J/T_c and a fixed value $J_1 = -1.0$.

Hence, in Fig. 12(a), for $J_1 = -1.0$, when $T = 0$ there are three well defined regions: the FM phase with $M = 1$, the FIM phase with $M = 1/3$, and the intermediate FRU phase; also, by increasing the temperature (for example, from $T = 0.1$ to 1.0) the disordered phase increases (the $|J|$ increases). Meanwhile, in Fig. 12(b), for $J_1 = 1.0$ and at zero temperature, we have a direct phase transition between the FM state and the FIM state. However, for a nearly zero temperature $T = 0.1$, a small intermediate region arises that corresponds to the disordered phase region. For higher temperature such as $T = 1.0$, the DP region is even larger.

Another way to analyze the total magnetization is by exploring the temperature dependence T/T_c of the total magnetization. In Fig. 13 we plot the magnetization as a function of temperature for two values of $J/T_c = \pm 1$ and $J_1 = -1.0$, where the magnetization of the saturated FM state and the FIM state is illustrated. For the case of $J/T_c = 1$ we have the FM region with $M = 1$ the total magnetization at zero temperature. The total magnetization vanishes at $T = T_c$ as temperature increases; therefore, a second-order phase transition occurs at the critical temperature.

For $J/T_c = -1$, the total magnetization corresponds to the FIM region, with $M = 1/3$ at zero temperature, and it vanishes at $T = T_c$ as displayed in Fig. 13. Thus a second-order phase transition occurs again at the critical temperature, which is in agreement with the critical point curve displayed in Fig. 7.

D. Entropy

The entropy can be easily obtained as a negative temperature derivative from the free energy (20) $\mathcal{S} = -\frac{\partial f}{\partial T}$, while the specific heat can be written as a temperature derivative from the entropy $C = T\frac{\partial \mathcal{S}}{\partial T}$. In what follows we consider only the case $J > 0$ since for $J < 0$ we have the same behavior.

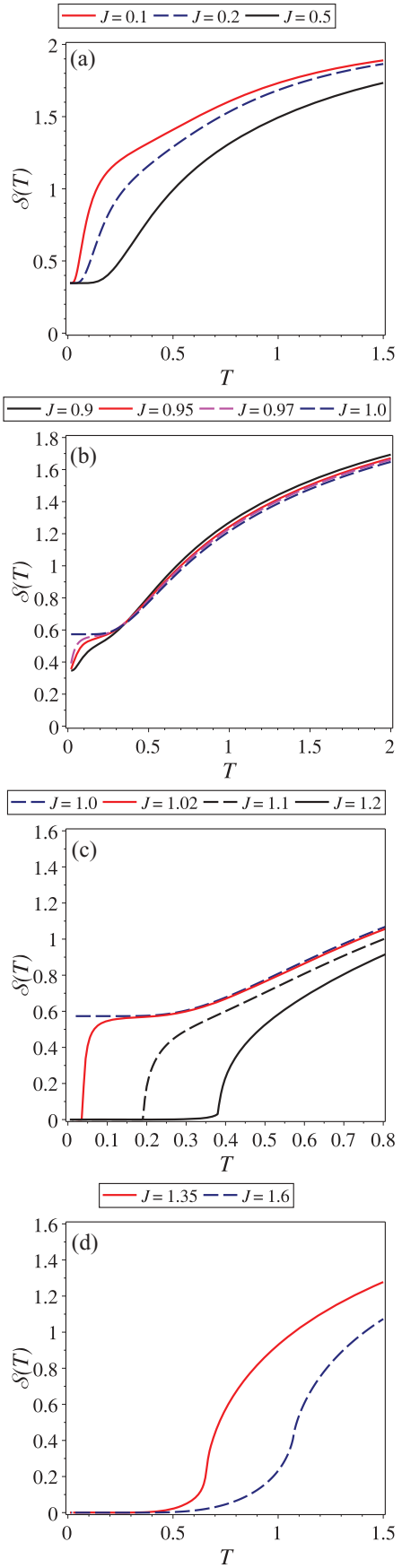

FIG. 14. (Color online) Entropy as a function of temperature for $J_1 = -1.0$ and (a) and (b) $J \leqslant 1$ and (c) and (d) $J > 1$.

In Fig. 14 we display the entropy as a function of temperature for several values of J with $J_1 = -1.0$ fixed. Figure 14(a) shows the low-temperature behavior of entropy, where the residual entropy appears at $\mathcal{S}_0 = \ln(2)/2 = 0.3465$ for $|J| < 1.0$. This means that we are in a geometrically frustrated region, which is in agreement with the illustration of the phase diagram in Fig. 2. The residual entropy is proportional to $\ln(2)$; this number comes from the two configurations given in Eq. (5). For $|J| = 1.0$ the residual entropy has a different nontrivial value as displayed in Fig. 14(b). To obtain the entropy explicitly, we return to Eqs. (21) and (22) and set $r_c = \frac{1}{u_c} = e^{-1/T_c}$. Thus we obtain

$$r_c^6 A(\phi) = \tfrac{5}{2} + \sqrt{2}\cos(\phi) + O\left(r_c^2\right)$$

and

$$r_c^{12} Q = \tfrac{1}{4} + \sqrt{2}\cos(\phi) + 2\cos^2(\phi) + O\left(r_c^2\right).$$

Finally, for $T_c \to 0$ ($r_c \to 0$) and using Eq. (20), the residual entropy becomes

$$\mathcal{S}_0 = \frac{1}{4\pi}\int_0^{2\pi} \ln\left[\frac{5}{2} + \left|\sqrt{2}\cos(\phi) + \frac{1}{2}\right| + \sqrt{2}\cos(\phi)\right] d\phi$$
$$\approx 0.573\,271\,475\,7. \tag{35}$$

This is due to the degeneration of the phase boundary between the FRU and FM (or FIM) regions at $T = 0$ (for details see Fig. 2). This result was derived in a way similar to that discussed by Wannier [26] for the case of a two-dimensional triangular lattice. While in Fig. 14(c) there is no residual entropy for $|J| > 1$, the standard temperature dependence of entropy appears with a strong change of curvature located at critical points where a second-order phase transition occurs.

It ought to be highlighted that in the low-temperature limit (below the critical temperature) the entropy (in the FM state) for $J > 1$ and with $J_1 = -1$ can be obtained from Eq. (20). More explicitly, by fixing $J = 1 + \delta$, where $\delta > 0$, it is possible to write $u = \frac{1}{rs}$, with $r = e^{-1/T}$ and $s = e^{-\delta/T}$. Substituting Eqs. (21) and (22) into Eq. (20), the integration

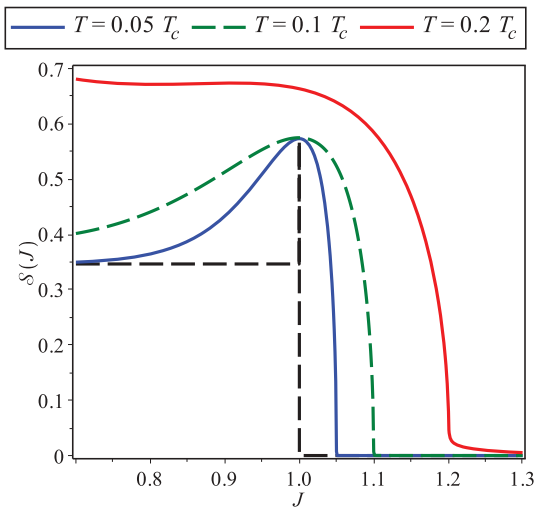

FIG. 15. (Color online) Entropy $\mathcal{S}$ as a function of the parameter J for a fixed low temperature and $J_1 = -1.0$.

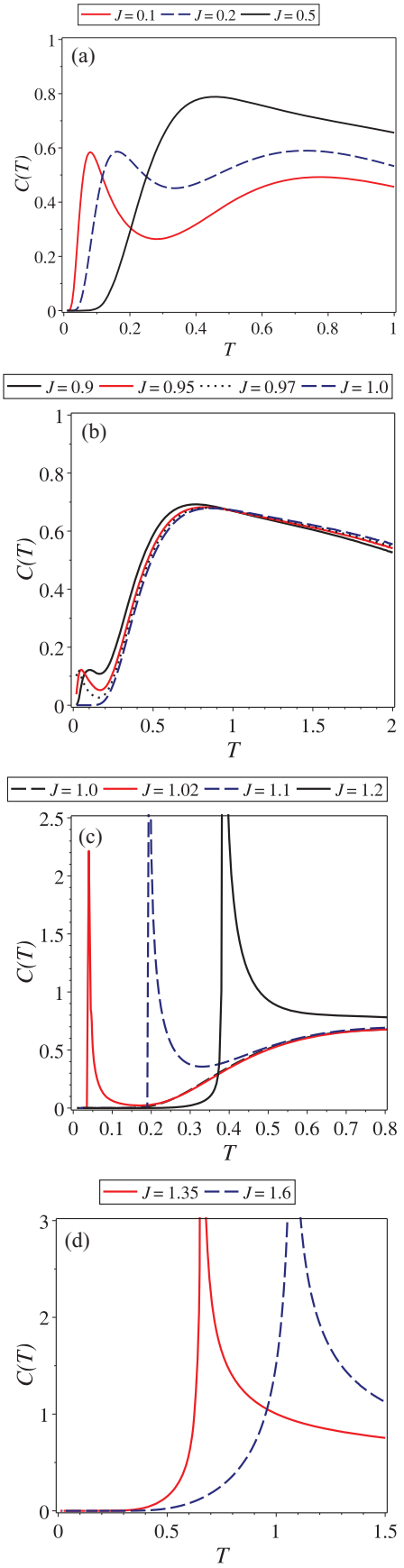

FIG. 16. (Color online) Specific heat as a function of temperature for $J_1 = -1.0$ and (a) and (b) $J \leqslant 1$ and (c) and (d) $J > 1$.

of Eq. (20) results in

$$f \approx -3 - 2\delta - T(-2\ln s + 2r^2 s^4)$$
$$\approx 1 - 4J - 2Te^{-2(2|J|-1)/T}.$$

Finally, the entropy $\mathcal{S} = -\frac{\partial f}{\partial T}$ can be written as

$$\mathcal{S} \approx \frac{2\Delta}{T} e^{-\Delta/T}, \tag{36}$$

where $\Delta \equiv 2(2|J| - 1)$ is the energy gap. In Figs. 14(c) and 14(d) the low-temperature limit is well fitted by the above limiting expression.

An additional plot of entropy $\mathcal{S}$ against J in the low-temperature limit is displayed in Fig. 15, where the residual entropy is illustrated by the dashed black line at zero temperature. For $J < 1$ there is residual entropy $\mathcal{S} = \ln(2)/2$, while for $J = 1$ the residual entropy becomes $\mathcal{S} = 0.573\,271\,475\,7$; for higher values of $J > 1$ there is no residual entropy. Thereafter, we observed the entropy in the low-temperature limit, where we can show the effects of residual entropy. The low-lying energy contribution for the entropy between the DP and the FM phase is absorbed by the second-order phase transition as a consequence of the entropy falling dramatically to zero entropy for $J > 1$; for higher temperature the entropy change curvature becomes softer.

E. Specific heat

Finally, we conclude our analysis of thermodynamics by exploring the temperature dependence of the specific heat. Some typical thermal variations of the specific heat of the pentagonal Ising model are plotted in Fig. 16 for several values of J and $J_1 = -1.0$ fixed. In Figs. 16(a) and 16(b) we present the temperature dependence of the specific heat in the DP states and show that there is no phase transition at finite temperature because we are observing the frustrated region. In Figs. 16(c) and 16(d) the specific heats are logarithmically divergent at the critical temperature, which is associated with a continuous phase transition between the spontaneously ordered and disordered phases. Clearly, this means that we are

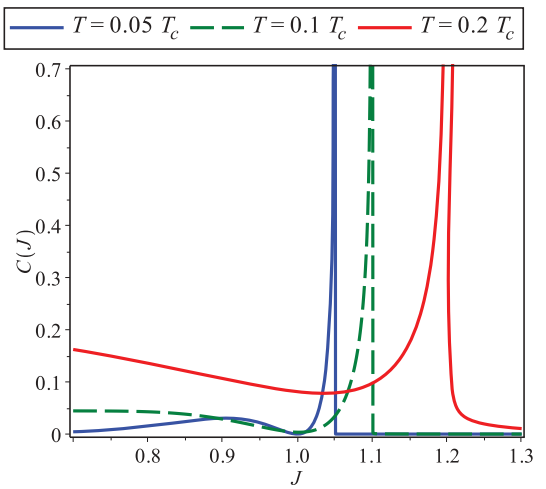

FIG. 17. (Color online) Specific heat as a function of J in the low-temperature limit and $J_1 = -1.0$.

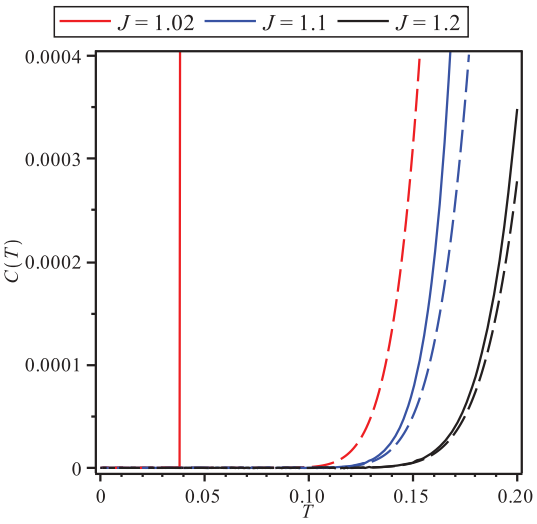

FIG. 18. (Color online) Low-temperature limit specific heat against temperature for the same values as in Fig. 16(c). The solid line corresponds to the exact specific heat and the dashed line is the low-temperature limit of the specific heat.

facing a FM region, which can be verified in the phase diagram illustrated in Fig. 2.

Plotted in Fig. 16(c) when $J \gtrsim 1$ and $J_1 = -1$ is the specific heat versus temperature; a surprisingly almost null specific heat is displayed, until the critical temperature is achieved. When the absolute value of the exchange interaction is only slightly above 1, the critical temperature (an order-disorder phase transition) can be obtained easily from Eq. (26); this critical temperature is approximately given by the expression

$$T_c \approx \frac{2(|J|-1)}{\ln(2\sqrt{2})} \tag{37}$$

in the low-temperature limit.

In Fig. 17 we display the specific heat as a function of J in the low-temperature limit, where we show the specific heat behavior around the second-order phase transition. As discussed previously, the low-lying energy contribution is absorbed by a second-order phase transition in the case of $J > 1$, while for $J < 1$ there is no second-order phase transition; then we can observe the low-lying energy contribution as a small anomalous broad peak.

Similarly, the low-temperature asymptotic limit for specific heat can be derived from Eq. (20) so that

$$C \approx \frac{2\Delta^2}{T^2} e^{-\Delta/T}. \tag{38}$$

The energy gap is large enough even when $J = 1.02$ because the order-disorder transition occurs for $|J| \approx 1 + \frac{T_c}{2}\ln(2\sqrt{2})$.

In Fig. 18 we show the magnification of Fig. 16(c) in low-temperature limit, which is well fitted by Eq. (38). The solid line corresponds to the exact specific heat and the dashed line represents the low-temperature asymptotic limit of the specific heat. For $J = 1.02$ the corresponding low-temperature approximation is valid for $T < 0.0385$, while for $J = 1.1$ and $J = 1.2$ clearly the low-temperature curve accompanies quite well the exact solution.

VI. CONCLUSION

Using the direct decoration transformation [16], we have solved the pentagonal Ising model with a more general coupling parameter and compared it with Urumov's [9] solutions. We have found a frustrated phase of the pentagonal Ising model.

In addition, we have obtained a simplified solution for the free energy, as well as a closed expression for the critical temperature. Although this model has already been solved by Urumov through the standard decoration transformation [10,17] in the nonfrustrated region ($J_1 > 0$), such a result contains unnecessary intermediate parameters that can be avoided so that a closed expression similar to Eq. (26) can be obtained. We have studied the ground-state phase diagram, which exhibits a ferromagnetic state, a ferrimagnetic state, and a frustrated state at $J_1 < -|J|$. Following the exact solution for the pentagonal Ising model, we have discussed the finite-temperature phase diagram, as shown in Figs. 8 and 9, identifying the phase transition between the FIM state and the DP state and also between the DP state and the FM state.

The analysis of the limits in Fig. 9 allows one to find three relevant phases. For $J_1 \to 0$ the pentagonal lattice reduces to a ferromagnetic (ferrimagnetic) decorated square lattice. For $J_1 \to \infty$ and $J > 0$ the pentagonal lattice reduces to the ferromagnetic square lattice. Finally, for $J_1 \to -\infty$ and $J < 0$ the pentagonal Ising model reduces to a ferrimagnetic square lattice. The total magnetization as a function of the parameter J and for a fixed value of J_1 for the ferromagnetic state ($M = 1$) and the ferrimagnetic state ($M = 1/3$) is shown in Fig. 12.

For a fixed value of $J_1 = -1$ there is a residual entropy $\mathcal{S}_0 = 0.3465$. For $|J| < 1.0$ and $|J| = 1.0$ a nontrivial residual entropy $\mathcal{S}_0 = 0.5732$ is found, as shown in Fig. 14. Because of the frustrated state, the entropy below the critical temperature shows a strong change of curvature for $J \gtrsim 1$. The specific heat capacity was also investigated at fixed $J_1 = -1$ and $|J| < 1$ [see Figs. 16(a) and 16(b)]. For $J_1 = -1$ and $|J| \gtrsim 1$ we have unusual behavior due to frustration of the entropy and the heat capacity at temperatures below the critical value, as shown in Figs. 16(c) and 16(d).

ACKNOWLEDGMENTS

M.R. acknowledges FAPEMIG for financial support. O.R. and S.M.d.S. thank CNPq and FAPEMIG for partial financial support.

[1] L. Onsager, Phys. Rev. **65**, 117 (1944).
[2] H. S Green and C. A. Hurst, *Order-Disorder Phenomena* (Interscience, New York, 1964).
[3] R. M. F. Houtappel, Physica **16**, 425 (1950); K. Husimi and I. Syozi, Prog. Theor. Phys. **5**, 177 (1950).
[4] I. Syozi, Prog. Theor. Phys. **6**, 306 (1951).

[5] T. Utiyama, Prog. Theor. Phys. **6**, 907 (1951).
[6] V. G. Vaks, A. I. Larkin, and Yu N. Ovchinni, Zh. Eksp. Teor. Fiz. **49**, 1180 (1965) [Sov. Phys. JETP **22**, 820 (1966)].
[7] F. Sun, X. M. Kong, and X. Ch. Yin, Commun. Theor. Phys. **45**, 555 (2006).
[8] M. H. Waldor, W. F. Wolff, and J. Zittartz, Z. Phys. B **59**, 43 (1985).
[9] V. Urumov, J. Phys. A: Math. Gen. **35**, 7317 (2002).
[10] M. E. Fisher, Phys. Rev. **113**, 969 (1959).
[11] E. Ressouche, V. Simonet, B. Canals, M. Gospodinov, and V. Skumryev, Phys. Rev. Lett. **103**, 267204 (2009).
[12] M. N. Iliev, A. P. Litvinchuk, V. G. Hadjiev, M. M. Gospodinov, V. Skumryev, and E. Ressouche, Phys. Rev. B **81**, 024302 (2010).
[13] T. Liu, Y. Xu, and C. Zeng, Mater. Sci. Eng. B **176**, 535 (2011).
[14] K. Jin, B. Luo, S. Zhao, J. Wang, and C. Chen, Chin. Phys. Lett. **28**, 087301 (2011).
[15] A. Ralko, Phys. Rev. B **84**, 184434 (2011).
[16] O. Rojas and S. M. de Souza, J. Phys. A: Math. Theor. **44**, 245001 (2011).
[17] O. Rojas, J. S. Valverde, and S. M. de Souza, Physica A **388**, 1419 (2009)
[18] J. Strecka, Phys. Lett. A **374**, 3718 (2010).
[19] J. Strecka, L. Canova, and M. Jascur, Phys. Rev. B **76**, 014413 (2007); A. Dakhama, Physica A **252**, 225 (1998).
[20] Y. L. Loh, D. X. Yao, and E. W. Carlson, Phys. Rev. B **77**, 134402 (2008).
[21] J. Strecka, L. Canova, M. Jascur, and M. Hagiwara, Phys. Rev. B **78**, 024427 (2008).
[22] J. S. Valverde, O. Rojas, and S. M. de Souza, Phys. Rev. E **79**, 041101 (2009).
[23] C. Fan and F. Y. Wu, Phys. Rev. B **2**, 723 (1970).
[24] T. C. Choy and R. J. Baxter, Phys. Lett. A **125**, 365 (1987).
[25] R. J. Baxter, Proc. R. Soc. London Ser. A **404**, 1 (1986).
[26] G. H. Wannier, Phys. Rev. **79**, 357 (1950).